



Simulation study on micro and macro mechanical behaviour of sand piles

Pradip Roul ^{a,*}, Alexander Schinner ^b

^a Institute for Numerical Mathematics, Duisburg-Essen University, D-47058, Duisburg, Germany

^b T-Systems, Dachauer Strasse 665, D-80995, Germany

ARTICLE INFO

Available online 5 August 2010

Keywords:

Discrete element method
Sand pile
Representative volume element
Stress
Strain
Fabric

ABSTRACT

We investigate numerically the micro and macro mechanical behaviour of non-cohesive granular materials, especially in the static limit. To achieve this goal we performed numerical simulations generating two-dimensional “sand piles” from several thousands of convex polygonal particles with varying shapes, sizes and corner numbers, using a discrete element approach based on soft particles. We emphasize that the displacement (strain) fields inside sand piles have not been measured in experiments on sand piles. Averaging is made reproducible by introducing a representative volume element (RVE), the size of which we determine by careful measurements. Stress tensors are studied for both symmetric and asymmetric sand piles in two-dimensional systems, where the particles are dropped from a point source. Furthermore, we determine the fabric tensor inside the sand piles. A surprising finding is the behaviour of the contact density in this kind of heap, which increases where the pressure is at a minimum. The fabric is linearly proportional to the product of the volume fraction and the mean coordination number for a pile consisting of mono-disperse mixture of particles. We observe that the macroscopic stress, strain and fabric tensors are not collinear in the sand piles.

© 2010 Elsevier B.V. All rights reserved.

1. Introduction

Granular materials are of fundamental importance and high interest to various branches of science and technology such as physics, applied mathematics and mechanics. In recent years, considerable interest in granular materials has been stimulated due to their high technological relevance: many products exist as a granulate at some stage of their processing history. Currently, a large amount of money is spent on the transportation and processing associated with the storage and containment of granular materials. However, about 50% of the money is unnecessarily spent because of problems related to the transport of the material from one part of the factory to another part of the factory.

Now, to have a look from another angle, it is often assumed that the side wall of a material container receives a constant force from the granular material inside. The common example of this issue is a model of a silo which is of great concern to various industries such as agricultural, pharmaceutical and mining industries, and all construction-based industries. However, this assumption is wrong, and in the general case, forces are non-uniformly propagated within the material, so they are also non-uniformly distributed at the wall of the silo. In some cases, if the force is much larger in some parts of the container than in other parts, the silo might collapse. For in order to

avoid problems such as the collapse or breach of a silo, one can simply increase the thickness of the walls by a generously chosen safety margin, which would be unnecessary if we had the knowledge how to design the silo in a proper way, especially taking into account the expected distribution of forces inside the silo. Therefore, the understanding of the basic physical principles behind the stress distribution in static granular materials is clearly important.

A simple example out of a collection of granular arrangements is the static sand pile. The formation of a sand pile is related to the fundamental behaviour of granular materials, including particle packing, segregation and pressure distribution [1–8]. The practice of storing granular materials in the form of sand piles occurs in many industrial situations dealing with particulate materials. Examples include the pharmaceutical industry relying on the processing of powders and tablets, the agricultural industry, coal industry and the food processing industries where seeds, coal (grain) and foods are transported and manipulated. Moreover, the storing of the material in a pile may be useful in fertilizer and mining industries. Thus, the flow of granular materials through a funnel (to form a pile) is an important problem for many industrial processes.

In order to handle the processing of granular materials in a pile properly, it is important to understand its mechanical properties. On the other hand, the study of deformation of granular materials either under external loading or unloading is also of practical importance for many industries. Although some progress has been made in this field during last ten years, these properties are still far from being exhaustively understood. Moreover, continuum models proposing constitutive

* Corresponding author. Tel.: +49 17620961836; fax: +49203 3792689
E-mail address: pradip.roul@uni-due.de (P. Roul).

relations to describe the flow and the deformation of granular materials have remained important, these constitutive relations are not able to completely describe the behaviour of granular materials.

This paper is organised as follows. In Section 2, we explain in briefly about the simulation method and how we construct a sand pile from a point source procedure. Section 3 constitutes the definitions and mathematical formulations of the macroscopic stress and fabric tensors as well as for the strain tensor, later using a best-fit approach. In Section 4, the introduction of representative volume elements (RVEs) used in the calculation of macroscopic continuum quantities is presented for the sand pile case. The results for various averaged macroscopic tensorial quantities obtained from discrete element method simulation for two-dimensional sand piles of soft convex polygonal particles are discussed in Section 5.

2. Simulation method

We simulate sand piles by building them from about of 6500 convex polygonal particles with varying shapes, sizes and edge numbers. The particles were poured from a funnel with a small outlet, known as “point source” procedure. When a pile is constructed from a point source, the particles are dropped always onto the apex of the sand pile and roll down the slopes of the pile. The number of polygon edges varies from six to eight for each simulation. The particles were inscribed into ellipses with uniformly distributed axes and were dropped onto the system from 0.5m height with initial velocity of 0.2m/s. The degree of poly-dispersity of the particles was about 30% and average size of the particles was 6.8 mm for both the major and minor axes of the ellipse. We used a static friction coefficient of $\mu = 0.54$ for the particles. The dynamic friction coefficient was same as that of the static friction coefficient. The density and Young's modulus of the particle were 5000kg/m^2 and 10^7N/m , respectively. The time step for simulating the sand piles was $2 \times 10^{-6}\text{s}$ and damping coefficient was used as $\gamma = 0.75$. The angle of repose obtained by taking the average over the left and right base angles of the sand piles, as it was about 28° .

A snapshot of one of the simulated sand piles constructed from a point source is illustrated in Fig. 1. The different shading corresponds to particles dropped at different times. We used a flat bottom ground plate. The walls and the funnel are made of immobile specially shaped particles and the bottom ground plate is fixed in shape as well. The characteristic properties of the ground plate, side walls and funnel are equal to the particles properties, which mean the Young's modulus of elasticity of the bottom ground wall is the same as for the particles, and the static friction coefficient between the bottom ground wall and the particles is the same as between the particles. In this work, we used a two-dimensional discrete element method (DEM) to compute the trajectory and rotational motion of each particle. DEM is a modeling technique for analyzing complex systems of individual particles and is used to simulate efficiently both quasi-static and dynamical behaviour of a large granular assembly. It has become a powerful numerical approach for analyzing non-homogeneous and discontinuous materials. It was originally proposed by Cundall et al. [9] for granular materials, especially in particle flow

simulation. Amongst various modeling techniques, DEM is the most realistic one for dynamical situations, because it explicitly takes into account the forces involved in the formation of assemblies of grains and in our case, also a realistic geometry of the particles.

DEM involves a molecular dynamics simulation with complex particles and force laws, including dissipation. The main difference between the discrete element method and preceding molecular dynamics methods lies in the particle interaction laws. Molecular dynamics simulations of atoms and molecules involve interactions with force laws that may be long range on the atomic scale, discrete element simulations involves inelastic interactions between particles and short range force laws, unless electrostatic forces are taken into accounts. In DEM approaches, the equations of motion describing the trajectories of particles are integrated numerically using a step by step integration procedure, often with a fixed time step. The basic structure of the DEM algorithm consists of a loop that contains the three steps:

- collision detection (at time t),
- force computation (at time t),
- solution of the equations of motion (integration process) (integrating up to time $t + \Delta t$).

We solve the equations of motion Eq. (1) for the forces acting on each particle and for the torques, using a fifth-order Gear predictor-corrector method [10], usually with a fixed time step.

$$m_i \ddot{r}_i = F_i + \sum_{j=1}^{n(i)} F_{ij} \quad (1)$$

$$I_i \ddot{\phi}_i = L_i + \sum_{j=1}^{n(i)} L_{ij}$$

Here, the subscript i runs over all the particles, $n(i)$ is the number of contact points of the particle i , and the subscript j runs over all the contacts of the particle i with other particles. F_i is the force acting on each particle i due to external fields, in our case this is only gravitation. F_{ij} is the sum of the normal contact force and tangential contact force as well as the dissipative force produced by the particle touching particle j in contact j .

In this study, we use soft but shape-invariant particles: two particles in contact with each other are allowed to interpenetrate partially. The normal forces are calculated from the overlap area and contact length defined as the distance between the two points of intersection of two overlapping particles, (defined in the appendix), whereas, the tangential force is calculated using a Coulomb type friction coefficient between particles. The dissipative normal force is calculated from the velocity during the time of overlap of particles using a phenomenological damping constant. The detailed descriptions of normal and tangential forces are given in [11].

3. Determining macroscopic quantities

In this section, we derive the mathematical formulas for various macroscopic tensorial field quantities including stress, strain, and fabric for sand piles consisting of polygonal particles. First we

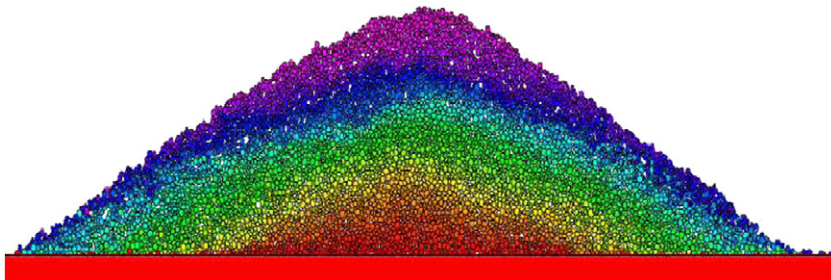


Fig. 1. Snapshot for a simulated sand pile constructed from a point source with 30% poly-disperse mixture of particles.

determine the formula of those tensorial quantities for a single particle and we then average over many particles by introducing a representative volume element (RVE).

3.1. Calculation of stress fields

In order to describe the behaviour of granular materials under external loading one has to determine macroscopic state variables like the stress through a proper averaging of microscopic variables. For the stress tensor, the microscopic variables are the forces acting between the particles and the lines connecting the centres of particles with their contact points, the so-called *branch vectors*. Once we have the forces and their points of contact, it is easy to derive a formula for the average stress obtained in a homogeneous polygonal particle assuming that the forces given in the contact points act on the corresponding edge of the polygon.

We derive the stress tensor in the following way: for a body in static equilibrium, the stress components at every point should satisfy the differential equation

$$\begin{aligned} \frac{\partial \sigma_{xx}}{\partial x} + \frac{\partial \sigma_{xy}}{\partial y} + F_x &= 0, \\ \frac{\partial \sigma_{yx}}{\partial x} + \frac{\partial \sigma_{yy}}{\partial y} + F_y &= 0, \end{aligned} \quad (2)$$

where F_x and F_y are the x and y components of the body forces per unit volume applied to the body. In the case of $F_x=0$ and $F_y=g_i$ (gravitation), the stress equilibrium Eq. (2) become

$$\begin{aligned} \frac{\partial \sigma_{xx}}{\partial x} + \frac{\partial \sigma_{xy}}{\partial y} &= 0, \\ \frac{\partial \sigma_{xy}}{\partial x} + \frac{\partial \sigma_{yy}}{\partial y} &= -g_i. \end{aligned} \quad (3)$$

The above expression (3) can be written in the form of

$$\frac{\partial \sigma_{il}}{\partial x_l} = g_i, \quad i = x, y \quad [g_x = 0, g_y = -g] \quad (4)$$

with an implied summation over subscript l (Einstein summation convention).

For the computation of the average stress tensor, we multiply both sides of the Eq. (4) by the coordinate x_j and integrate over the "volume" V^p of the particle p .

$$\int_{V^p} x_j \frac{\partial \sigma_{il}}{\partial x_l} dV^p = \int_{V^p} x_j g_i dV^p, \quad (5)$$

The left hand side of Eq. (5) can be recast as follows:

$$\begin{aligned} \int_{V^p} x_j \frac{\partial \sigma_{il}}{\partial x_l} dV^p &= \int_{V^p} \frac{\partial (\sigma_{il} x_j)}{\partial x_l} dV^p - \int_{V^p} \sigma_{il} \frac{\partial x_j}{\partial x_l} dV^p \\ &= \int_{V^p} \frac{\partial (\sigma_{il} x_j)}{\partial x_l} dV^p - \int_{V^p} \sigma_{il} \delta_{jl} dV^p \\ \int_{V^p} x_j \frac{\partial \sigma_{il}}{\partial x_l} dV^p &= \int_{V^p} \frac{\partial (\sigma_{il} x_j)}{\partial x_l} dV^p - \int_{V^p} \sigma_{ij} dV^p. \end{aligned} \quad (6)$$

The right hand side of Eq. (5) is

$$\int_{V^p} x_j g_i dV^p = g_i \int_{V^p} x_j dV^p = 0. \quad (7)$$

(since $\int_{V^p} x_j dV^p = 0$, as x_j is measured from the centre of mass).

Inserting Eqs. (6) and (7) in Eq. (5) yields

$$\begin{aligned} \int_{V^p} \frac{\partial (\sigma_{il} x_j)}{\partial x_l} dV^p - \int_{V^p} \sigma_{ij} dV^p &= 0 \\ \Rightarrow \int_{V^p} \frac{\partial (\sigma_{il} x_j)}{\partial x_l} dV^p - V^p \langle \sigma_{ij}^p \rangle &= 0 \\ \Rightarrow \langle \sigma_{ij}^p \rangle &= \frac{1}{V^p} \int_{V^p} \frac{\partial (\sigma_{il} x_j)}{\partial x_l} dV^p. \end{aligned} \quad (8)$$

By applying the divergence theorem to Eq. (8), the volume integral can be transformed into a surface integral. This gives

$$\langle \sigma_{ij}^p \rangle = \frac{1}{V^p} \int_{S^p} x_j \sigma_{il} n_l dS^p. \quad (9)$$

$\sigma_{il} n_l = F_i$ is the traction along the surface element dS^p , a force per area, in 2D per length.

If the surface force on edge C is considered constant along the edge, we have $\sigma_{il} n_l \Delta S^C = F_i^c$ for that edge.

Hence the right hand side of the Eq. (9) can be written as the sum over all contact forces.

$$\langle \sigma_{ij}^p \rangle = \frac{1}{V^p} \sum_{c=1}^p x_j F_i^c. \quad (10)$$

Since in the void space of the averaging volume element there is no stress, we just need to determine the average stress tensor over all particles whose centre of mass lies inside the averaging volume element V

$$\langle \sigma_{ij} \rangle = \frac{1}{V} \sum_{p=1}^n V^p \langle \sigma_{ij}^p \rangle. \quad (11)$$

Inserting Eq. (10) in Eq. (11) we obtain a double sum given by the expression:

$$\langle \sigma_{ij} \rangle = \frac{1}{V} \sum_{p=1}^n \sum_{c=1}^p x_j F_i^c. \quad (12)$$

Eq. (12) allows us to determine the averaged stress tensor over many polygonal particles in an averaging volume element V . We can now define the stress tensor (from Eq. (12)) as the dyadic product of the contact force F^c acting at the point c with the corresponding branch vector x^c , as schematically shown in Fig. 2.

3.2. Calculation of strain fields

To a certain extent, even more interesting than to study the stress tensor is to determine the strain distribution under a sand pile. Since our study is concerned with the sand pile model, first we have to deform (relax) the sand pile in the proper way in order to obtain realistic results for the strain tensor within the sand pile. One might regard it as one of the essential questions in the field of granular heaps, how deformation under stress can be defined, aiming at the identification of a strain tensor. As of now, no strains have been measured in experiments on sand piles, and continuum models assume that for sand piles displacement fields are not available. Therefore, several closure relations proposed for the equations describing sand piles have been obtained without making use of the strain tensor [1–3].

To obtain a measure for strain numerically, the sand pile is allowed to relax under reduction of gravity. We reduce gravity for a pile slowly by about 10% from the actual state (ambient gravity level) of the pile at $g=9.81$, this will lead us to obtain strains by determining the

position changes at the particle centres when gravity was changed from one level to the other and by using these as displacement vectors for the calculation of a Cambou's best fit strain.

3.2.1. Cambou's best-fit strain

In order to determine the strain fields inside the sand piles, we use one of the simplest techniques, namely the best-fit strain of Cambou et al. [12] who consider the relative translation of the particles. Let us assume that two grains p and q have a contact c and du_j^p denote the translation of the centre of particle p . The relative translation of the pairs of grains p and q forming contact c is

$$d\Delta u_j^c = du_j^q - du_j^p. \tag{13}$$

The vectors r_i^{pc} and r_i^{qc} connect the corresponding particle centres to the contact point c , as illustrated in Fig. 3 and are what we called branch vectors so far. According to Cambou et al. the branch vector assigned to a contact is defined as $l_i^c = r_i^{pc} - r_i^{qc}$, i.e., it is simply the difference of the centre-of-mass vectors of the two particles sharing the contact c .

According to Cambou et al., the solution of best-fit translation gradient tensor ϵ_{ij} is

$$\epsilon_{ij} = z_{ik} \sum_c d\Delta u_j^c l_k^c \tag{14}$$

$i, j, k = x, y$ summation over k implied). Where z_{ij} denotes the inverse of

$$\text{matrix} \begin{pmatrix} \sum_{c=1}^n l_x^c l_x^c & \sum_{c=1}^n l_x^c l_y^c \\ \sum_{c=1}^n l_x^c l_y^c & \sum_{c=1}^n l_y^c l_y^c \end{pmatrix} = \begin{pmatrix} z_{xx} & z_{xy} \\ z_{yx} & z_{yy} \end{pmatrix} \text{ for two-dimensional systems.}$$

The components of the strain tensor in two-dimensions are as follows

$$\epsilon_{xx}(x, y) = \sum_c d\Delta u_x^c (z_{xx} l_x^c + z_{xy} l_y^c)$$

$$\epsilon_{yy}(x, y) = \sum_c d\Delta u_y^c (z_{yx} l_x^c + z_{yy} l_y^c)$$

$$\epsilon_{yx}(x, y) = \sum_c d\Delta u_x^c (z_{yx} l_x^c + z_{yy} l_y^c)$$

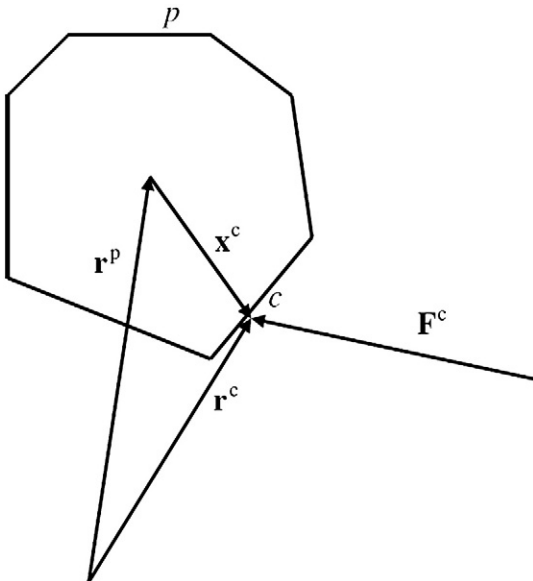


Fig. 2. Schematic plot of a particle p with branch vector x^c and the position vector r^p . The branch vector x^c points from the centre of mass of the particle p to contact point c .

3.3. Fabric tensor

A particular quantity that describes the internal texture of the granular assembly is known as the fabric tensor. Several definitions are available to define the fabric tensor inside an assembly of grains, see in Refs. [13–20]. Using the contact points of the individual particles, we can calculate the fabric tensor for single particle. Then it is easy to derive the formula for the average fabric tensor over sufficiently many particles in an averaging volume element.

3.3.1. The fabric tensor for one particle

The formula for the fabric tensor of particle p is given [13,14] by

$$F_{ij}^p = \sum_c n_i^c n_j^c, \tag{15}$$

where n_i^c is the i th component of the unit vector to contact point c of the considered particle p , as shown in Fig. 4.

$$n_x^c = \frac{x_c - x_p}{\sqrt{(x_c - x_p)^2 + (y_c - y_p)^2}},$$

$$n_y^c = \frac{y_c - y_p}{\sqrt{(x_c - x_p)^2 + (y_c - y_p)^2}}, \tag{16}$$

where (x_c, y_c) and (x_p, y_p) are the contact point and the centre of mass, respectively, and the sum in Eq. (15) is over all the contacts of the particle p . The trace of the fabric tensor then determines the number of contacts of particle p

$$\text{tr}(F_{ij}^p) = \sum_c n_i^c n_i^c = C^p. \tag{17}$$

3.3.2. The fabric tensor for many particles

We take an average over many particles in a averaging volume element V to determine the average fabric tensor. The averaged fabric tensor over many particles is given by

$$\langle F_{ij} \rangle V = \frac{1}{V} \sum_p V^p F_{ij}^p, \tag{18}$$

where V is the volume of the averaging element that contains the particles whose centre of mass lies inside it and V^p and F_{ij}^p respectively denote the volume and the fabric tensor of particle p .

3.3.3. Coordination number

The average coordination number C , in our definition, corresponds to the mean number of contacts per particle within a volume element V , is given by

$$C = \frac{1}{N} \sum_{p \in V} n^p, \tag{19}$$

where n^p denote the number of contacts of the particle p and N is number of particles that lie within the averaging volume element V whose centres of mass lie inside it.

4. Averaging procedure

One can obtain detailed information about measurable quantities such as forces, stresses, and displacements of an individual particle from the discrete element simulation. However, the behaviour of an individual particle is not significant for the behaviour of the whole system, as most of the measurable microscopic quantities in granular material vary strongly as a function of position.

In this regard, one common example is the stress tensor, which is not constant across grains (microscopic level), but usually it shows its largest values for particles with a large number of contacts. Moreover, the microscopic stress tensor would not be a convenient means to describe the macroscopic sand pile, as it fluctuates widely within a volume containing a few sand grains. In fact, it is zero in the voids between grains. Hence for a continuum description, we need to average microscopic quantities over suitable domains, which will reduce the relative fluctuations. In order to suppress the fluctuations, we need to perform averages over sufficiently many particles in an averaging volume element. But, the question is how many particles are actually required to determine the average macroscopic tensorial quantities, which means, one has to determine the number of particles (or appropriate size of the volume element) providing realistic results for the macroscopic quantities including fabric, strain, stress and volume fraction of the sand pile.

In our work, averages are performed by introducing a representative volume element (RVE) via the requirement that the average becomes size independent, if the volume is taken equal to this value or larger. Averaging over different volumes gives different results, as long as the volume element is too small. As we increase the size of the volume element in the computation of the average, the averaged quantity converges to a certain value. A size of the volume element near but above the minimum needed for convergence gives the representative volume element to be used in evaluations of macroscopic fields.

We have taken into account those particles whose centres of mass lie inside the averaging volume element to determine the macroscopic quantities. Sometimes, this method is referred to as the particle centre averaging technique.

The simulation results for the individual components of the strain tensor against the number of particles are displayed in Fig. 5. The number of particles shown in the graph corresponds to the size of the volume element. It can be seen in the figure that all the components of the strain tensor are converged approximately at the same number of particles. We find that a size of the volume element containing 100–200 particles is sufficient to serve as RVE.

On the other hand, we determine the size of the RVE for the fabric tensor as illustrated in Fig. 6. We find from the figure that the size of the volume element is the same as for the strain tensor. It should be noted that the size of the volume element that we consider for the calculation of the fabric and strains is same as for the stress and volume fraction of the sand pile.

5. Simulation results

The simulation result of averaged density (volume fraction) at different heights inside a symmetric sand pile created from a point source is represented in Fig. 7. The figure demonstrates the density

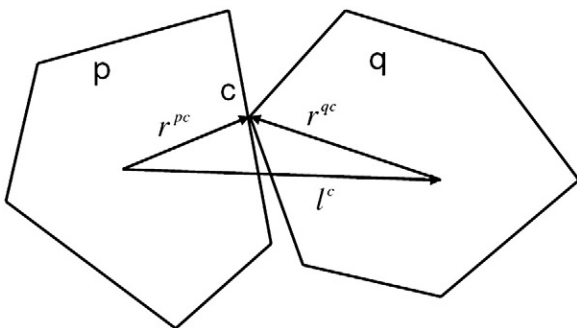


Fig. 3. Schematic diagram of Cambou's branch vector F assigned to the contact c of two particles. Note that according to our preceding nomenclature r^{pc} and r^{qc} are the branch vectors.

changes with relative heights inside a sand pile and the middle region of the pile shows a higher density than the rest of the sand pile. The middle region has a density that is approximately 8–10% higher than the density in the vicinity of the free surface of the sand pile.

Next we determine in the following some properties of the fabric tensor inside a sand pile. The simulation result of the trace of the averaged fabric tensor, describing the average contact density of the sand pile, derived by taking the sum of the major and minor eigen values of the fabric tensor, at different heights of the piles is illustrated in Fig. 8A. The figure demonstrates that the mean number of contacts increases towards the centre and towards the bottom layer and decreases towards the surface and towards the top layer of the pile. We observe that the number of contacts of the particle is higher where the density is maximum. We then determine the deviatoric fraction of the fabric, defining the degree of anisotropy in the contact network of the sand pile, as simulation results shown in Fig. 8B. It can be seen in the figure that the deviatoric fraction decreases towards the centre and increases towards the free surface of the pile that lead to conclude that the fabric is much more isotropic in the central core region of a sand pile than in the outer part. The angle of the orientation of the major eigenvector of fabric tensor with respect to the horizontal axis is given in Fig. 8C at different heights inside the sand pile. We find that the orientation of the fabric changes from -40° (left) to $+40^\circ$ (right).

The averaged stress tensor was evaluated throughout the sand pile; typically, we represent it via a plot of stress tensor components as a function of the lateral coordinate x of the pile for layers of given heights y_1, y_2, \dots, y_n . The stress tensor is normalized by the hydrostatic static pressure, ρgh , where the quantities ρ and h denote the density and the height of the sand pile, respectively, and g is the acceleration due to gravity. In order to suppress the fluctuations of the result of stress tensor for single sand pile, we have taken average over 14 sand piles. The averaged vertical normal stress tensor (pressure) obtained from DEM simulation is displayed in Fig. 9A. We find that the vertical normal stress distribution changes with the vertical position in the sand pile. We find a pressure dip below the apex of the sand pile which appears not only at the bottom layer of the sand piles but also exists up to a certain height inside sand piles (but not above). It is a somewhat surprising result that for a sand pile constructed from a point source the density is maximum at the centre where the pressure is actually *minimum*. An increase of density with decreasing pressure is a signature of instability. A qualitative explanation of the pressure minimum would be a local collapse of the grain arrangement in the interior, leading to increased density and an 'arch' of particles above the collapsed part supporting the weight of the column of grains below the pile tip.

The simulation result of anisotropy stress is illustrated in Fig. 9B. At the centre it is about 0.2, at the flanks it is 0.45 and closer to the surface it increases to 0.6 (approximately). The orientation of the major eigenvector of stress tensor is given in Fig. 9C at different heights inside the pile. It changes from -30° (left) to $+30^\circ$ (right). Moreover, there is a well known macroscopic approach named "Fixed principal axes" (FPA) model [3] based on an analytic description for describing the stress distribution under a sand pile. The closure relation of the FPA model can be derived more intuitively by assuming that the principal axes of the stress tensor take the fixed directions $\pm\psi$ on both sides of the central axis of the sand pile, where $\psi = (\pi - 2\phi) / 4$, hence the name of the model is FPA. ϕ is the angle of repose of the sand pile. Moreover, the FPA model leads to a pronounced dip in the pressure distribution under the tip of the sand pile, as we observed qualitatively similar behaviour in the pressure profile obtained from our simulation illustrated in Fig. 9A. However, the conclusion of FPA model does not correspond well to our simulations – the orientation of the stress tensor is not constant throughout the sand pile, as one can see in Fig. 9C.

We have represented and discussed above numerical results concerning the stress distribution inside the symmetric sand piles. Up to now, no stresses have been measured for asymmetric sand piles either experimentally or numerically. However, there exists in the

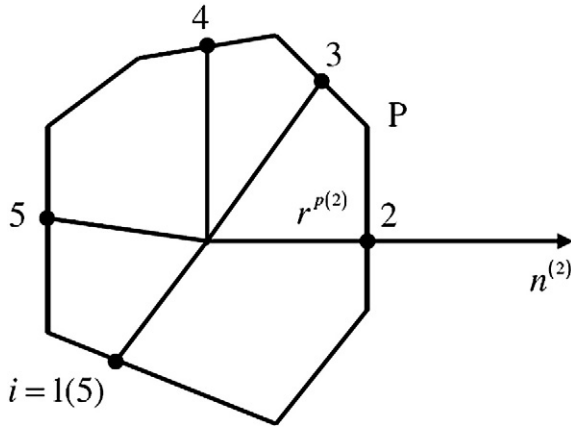


Fig. 4. Schematic plot of a polygonal particle with five contact points. The branch vector $r^{p(c)}$ and the unit vector $n^{(c)}$ are shown at contact point $c = 2$.

literature an elasto-plastic continuum model set up by Didwania et al. [2] predicting an analytical solution for the stress distribution inside an asymmetric sand pile.

In order to determine stresses under an asymmetric sand pile we have performed discrete element method simulation of two-dimensional asymmetric sand piles. We simulate asymmetric sand piles by constructing them from about of 3900 polygonal particles that are poured from a point source. One of the simulated sand piles is shown in Fig. 10. We used a poly-disperse mixture of round of particles with a degree of poly-dispersity of about 25%. The procedure for constructing an asymmetric sand pile from a point source is essentially the same as that of the construction of a symmetric sand pile, but instead of using a fixed height point source (the funnel), we move the funnel slowly horizontally towards the right hand side. The average angle of repose for the left-hand side of the sand pile obtained for seven sand piles was 28° and it was 21° for the right-hand side of the sand pile. Fig. 11 reveals the simulation results for the averaged normalized vertical normal stress tensor along horizontal cuts at different heights of an asymmetric sand pile. In the figure, circles symbols connected by line represents the results at the bottom layer of the corresponding sand pile, whereas the stars symbols corresponds to the top layer. We find that there is an asymmetric pressure distribution below the apex of the pile, and a dip exists in the stress profile. We note that the behaviour obtained using the DEM simulation is same as that of the theoretical prediction obtained by Didwania et al, see in Ref. [2].

Next, we focus on the sensitivity of the strain distribution (total strain) to the preparation of sand piles. Before interpreting the results for the strain tensor, first, we present simulation results for the movement of each individual grain inside the sand pile under gravity reduction. The result obtained from the simulation is represented in Fig. 12. Each arrow shown in the figure corresponds to the movement of an individual particle. The arrow is drawn from the initial position of the centre of mass (x_i, y_i) of the particle i at the ambient gravity level of a sand pile at $g = 9.81 \text{ m/s}^2$ towards the final point of the centre of mass (x'_i, y'_i) at the new state of the sand pile obtained by reducing gravity slowly by about 10%. As expected, the range of movement of a particle decreases towards the bottom layers of the sand pile, and increases towards the surface and the tip of the sand pile.

The averaged vertical normal strain tensor component u_{yy} obtained from DEM simulations is displayed in Fig. 13. The topmost curve in the graph shows the strain tensor result at the bottom layer of the corresponding sand pile, whereas the bottom curve corresponds to the top layer. Heights are given as function of the total height of the pile to its apex. An interesting feature of the vertical normal strain tensor for various heights is that the vertical normal strain changes with the layer position in the sand piles like the stress tensor. The

averaged vertical normal strain shows a dip near the centre of the piles. It can be seen that the strain dip appears not only at the bottom layer but also exists up to the certain height inside the sand pile. The orientation of the strain tensor with respect to the horizontal axis is given in Fig. 14. It changes from -45° (left) to 45° (right).

Moreover, the orientation of three macroscopic tensors stress, strain and fabric are plotted in Fig. 15 only for the first two bottom layers of the pile. It can be seen, however, that the orientations are different for three tensors, which means that these macroscopic tensors are not collinear. Most likely this limits the utility of a description of granular piles in terms of isotropic elasticity.

In the next step, we determine the correlation between trace of the fabric tensor and product of the volume fraction v and the mean coordination number C . We plot the product of the volume fraction and mean coordination number of a sand pile as a function of the trace of the fabric tensor in Fig. 16. The top panel of the figure shows the result for a mono-disperse arrangement of particles, whereas the bottom panel shows the same for a poly-disperse mixture of the particles. In the first case, all the data points collapse on a single straight line, which means that the averaged fabric tensor is linearly proportional to the product of the volume fraction and mean coordination number. Moreover, the proportionality constant is one, i.e.,

$$\text{tr}(\langle F \rangle) \cong vC. \quad (20)$$

This is to be expected from the definition of the fabric tensor. Remember that for a single particle $\text{tr}(F) = c^p$ (Eq. 17).

On the other hand, for a poly-disperse systems the trace of the averaged fabric tensor is not linearly proportional to the product of the volume fraction and mean coordination number: i.e.

$$\text{tr}(\langle F \rangle) \neq vC. \quad (21)$$

This is not unexpected either, because for poly-disperse particles the local volume fraction differ and we have $vC \neq \langle v c^p \rangle$, meaning that volume fraction and contact number are not statistically independent. For poly-disperse granular materials, Madadi et al. [21] introduced a dimensionless (scalar) factor, the so-called “correction factor” which is only dependent on the particle size probability distribution function in order to predict a macroscopic material property based on a microscopic property of the granular materials. According to Madadi et al, the trace of the fabric tensor can be factorised into three contributions: (1) the volume fraction of the granular assemblies (2) the mean coordination number (3) a correction factor g_2 . We can write the trace of the averaged fabric tensor for a poly-disperse granular system as in a mathematical expression:

$$\text{tr}(\langle F \rangle) \cong vCg_2. \quad (22)$$

We have determined the correction factor g_2 simply from our DEM numerical simulation results by taking the ratio between $\text{tr}(\langle F \rangle)$ and vC , i.e.

$$g_2 = \frac{\text{tr}(\langle F \rangle)}{vC}. \quad (23)$$

From the above Eq. (23), we find the correction factor $g_2 = 1.045$ for a sand pile consisting of poly-dispersity mixture of the particles with a degree of poly-dispersity of 30%.

We then plot in Fig. 17, the trace of the fabric tensor against the volume fraction of a sand pile. The behaviour is roughly linear, meaning that the contact number density is proportional to the volume fraction of the sand pile. In conclusion, we have a lower pressure in the central

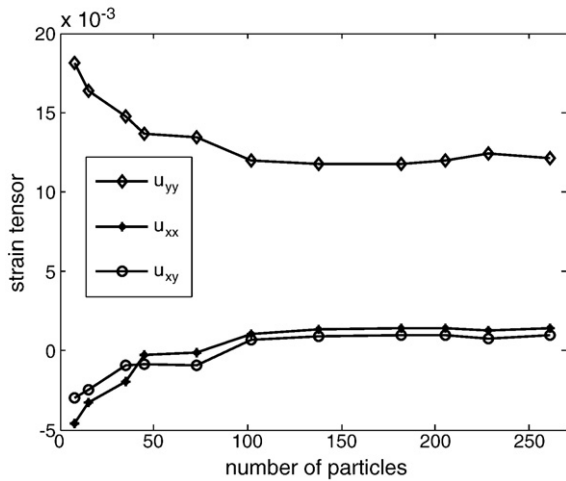


Fig. 5. Representative volume element for strain tensor.

region of the sand pile than in the region around, the density is locally maximum and the contact-number-density shows same behaviour.

6. Conclusions

As a first step of this work, several microscopic quantities including forces, contact points, contact displacement, and displacement of the particle centres of sand pile were evaluated, with the aim to determine from them averaged macroscopic variables, viz. stress, strain, density, and fabric. To obtain macroscopic quantities from microscopic ones averaging was performed on “representative volume elements” (RVEs) in computing the macroscopic variables for a continuum description. A sufficient size for an RVE to yield converged results was determined to contain 100–200 particles.

The pressure distribution was evaluated both for symmetric and asymmetric sand pile created by pouring materials from a point source. We find, not unexpectedly, that the pressure is not only minimum at the bottom layer, but also in higher layers of the pile. However, it disappears in layers near the tip of the sand pile. The density profile of sand piles was also measured; we observe that the middle region of the sand piles constructed from a point source displays higher density than the rest. In conclusion, the averaged density is maximum in the centre of the piles where the pressure is minimum. Furthermore, we found an asymmetric pressure distribution inside the asymmetric sand piles and a dip in the pressure profile beneath the tip of the piles. The authors in Ref. [2] were assumed a similar behaviour.

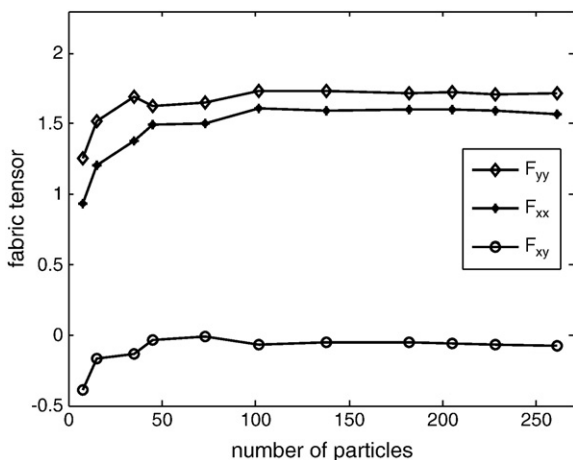


Fig. 6. Representative volume element for fabric tensor.

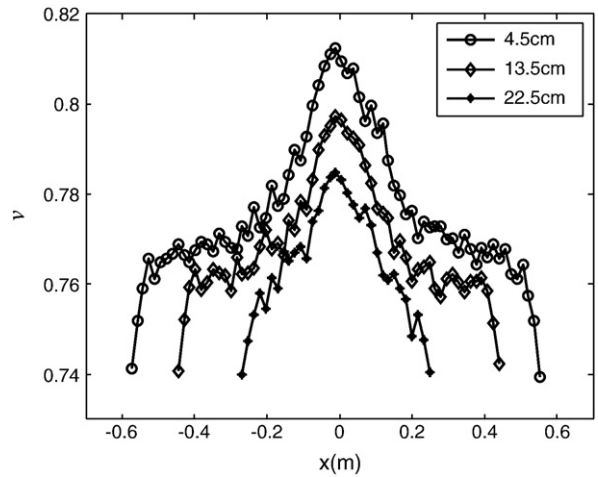


Fig. 7. Volume fraction ν for a sand pile constructed from a point source.

We have measured numerically the strains inside the sand piles. It is to be noted that it may be difficult or impossible to determine this tensorial quantity in experiments. Knowing this distribution will lead to a better understanding of the processes happening inside a granular assembly. In particular, we showed that it is possible to obtain not only stresses but also displacements in the heap, by judicious use of an adiabatic relaxation experiment, in which gravity is slowly changed. From the measurements, we find that the vertical normal strain u_{yy} is not only minimum at the bottom layer, but also in higher layers of the sand piles like the stress tensor. The behaviour what we observed for the strain tensor is same as that for the stress tensor.

Additionally, we determined numerically the fabric tensor in order to describe the internal texture of granular assemblies. This will lead to a measure of the degree of the internal anisotropy of the assemblies of grains and provides as with the number density of the particle contacts within the granular system. The fabric tensor was obtained using normalized branch vectors at the contact points of the particle. The trace of the averaged fabric tensor was measured throughout the sand pile, with the result that the number of contacts of the particles increases towards the centre and decreases towards the free surface of the sand pile. Since the density is maximum in the centre for the sand pile constructed from a point source, this means that the number of contacts is higher where the density is maximum, as expected. We observe that the deviatoric fraction of the fabric tensor decreases towards the centre, which means the fabric is more isotropic near the centre of the sand pile and more an-isotropic in the outer part.

Furthermore, we conclude that the trace of the averaged fabric is linearly proportional to the product of the volume fraction and the average coordination number for a pile consisting of a mono-disperse mixture of particles, whereas it turns out to be incorrect for a pile consisting of a poly-disperse mixture of particles.

An essential observation is that the macroscopic tensors stress, strain and fabric are not collinear in the granular heap, i.e. their orientations are different. The orientation of the fabric is tilted most, that of the strain tensor is tilted least and thus, simply speaking the material cannot be described by a simple elastic model involving only two elastic constants. However, in the case where there is a strong deviation between the local orientation of the fabric and stress tensors, the fabric tensor has almost equal eigen values, rendering a precise determination of its principal axes difficult. Hence, more work needs to be done to determine whether this deviation is significant. In the case of elliptic particles, all three tensors seem to be well aligned with each other.

As an outlook, simulation results of stress and strain tensor may serve for a determination of nonlinear stress-strain relationships for sand piles. Moreover, the constitutive relations proposed for the sand pile model so far are in terms of the stress tensor only and it would be

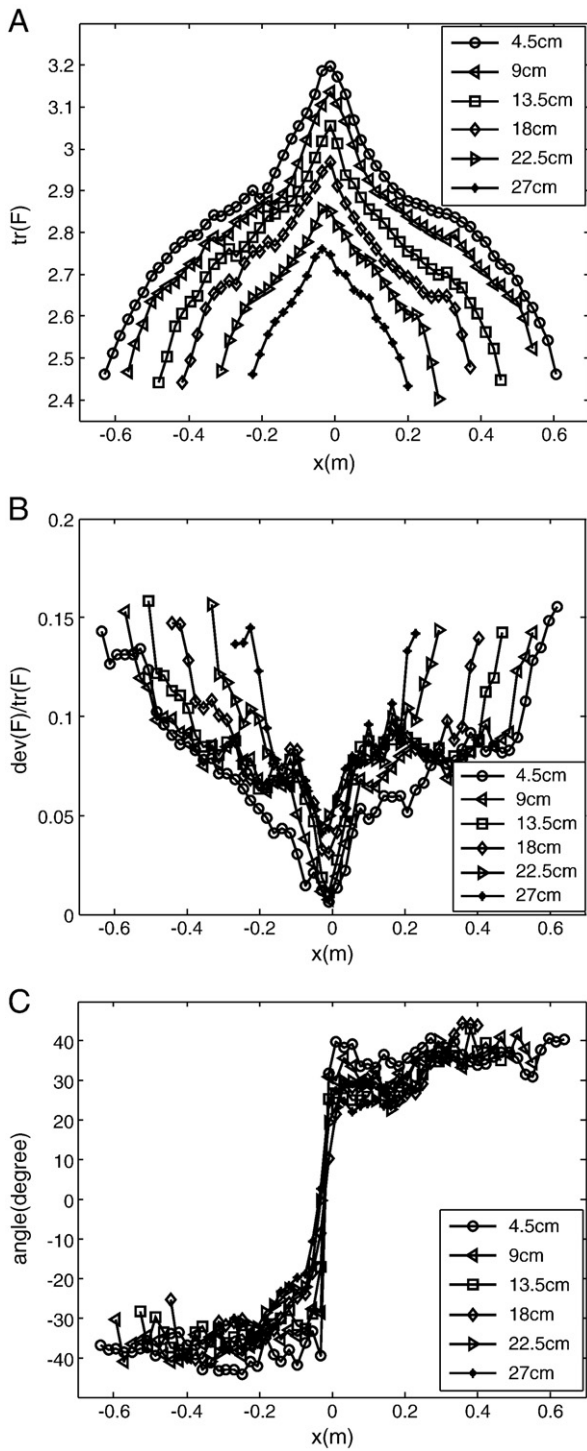


Fig. 8. A–C: Simulation results of the different properties of the averaged fabric tensor for a sand pile. (A) Trace of the fabric tensor, (B) deviatoric fraction of fabric, and (C) orientation of fabric versus lateral position in the sand pile.

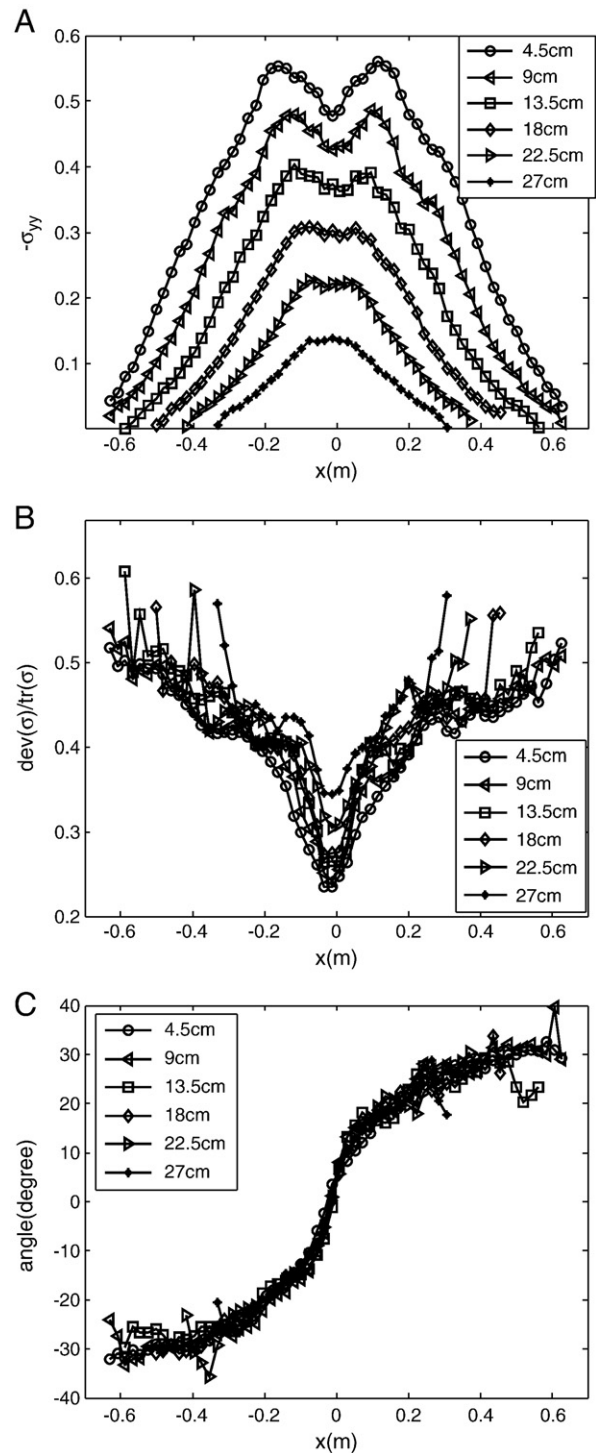


Fig. 9. A–C: Plot of A. Vertical normal stress tensor σ_{yy} , B. Deviatoric fraction of stress σ . Orientation of stress tensor at different heights inside the sand pile.

interesting to develop better constitutive relations using not only the stress and strain tensor, but also the density and or the fabric tensor to get a set of fully working continuum equations.

Acknowledgements

We are grateful to Prof. Klaus Kassner and Prof. Stefan Luding for providing us valuable suggestions on the computational results. We

would like to acknowledge the Deutsche Forschungs-gemeinschaft (DFG) for providing financial support.

Appendix A. Force calculation

In this study, we use soft but shape-invariant particles. In principle, if using soft particles, one should allow them to deform on contact. The size, direction and point of application of the force are calculated

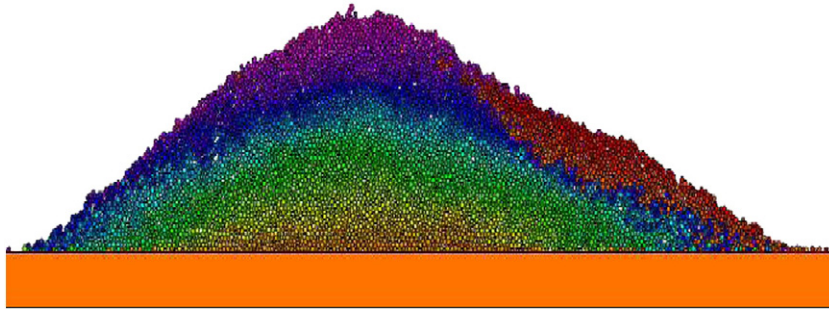


Fig. 10. Snapshot for a simulated asymmetric sand pile constructed from a point source.

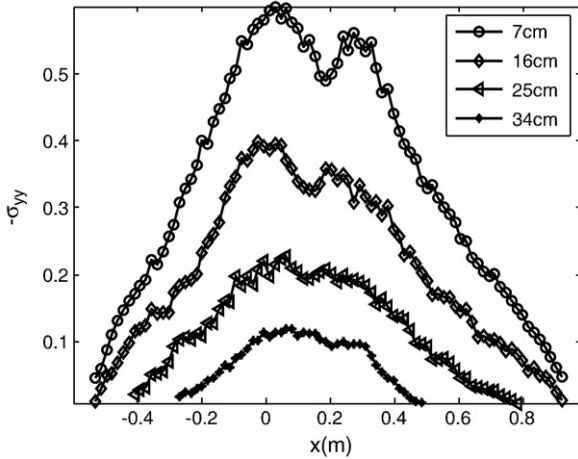


Fig. 11. Vertical normal stress distribution σ_{yy} at various heights inside a two-dimensional asymmetric sand heap constructed from a point source.

from the geometric characteristics of the overlap area and contact length using the relative velocity of the two particles. The repulsive force between two particles is increased when the area of overlap becomes larger. Therefore, in a real simulation, the overlap always remains small in comparison with the particle extension.

A.1. Normal force

Normal forces are supposed to act in the normal direction of the particle contacts. Fig. 18 displays a pair of overlapping particles namely i and j . Each force acts at a contact point between two particles. In general, the direction of the force will not point towards the centre of mass of the particle.

The normal force F_{\perp} can be decomposed into two parts, namely the repulsive normal force R_{\perp} and the dissipative normal force D_{\perp}^* , i.e. it can be written as

$$F_{\perp} = R_{\perp} + D_{\perp}^*$$

The point of contact denoted as s_{ij} in which the contact forces are applied, is determined as the centre of the line of contact, joining the two intersection points p_1 and p_2 of the polygons. Here r_i and r_j are the vectors from the centre of mass of the respective particles to the centre of the contact line.

In a way, the most important force is the repulsive normal force which is taken proportional to an effective interpenetration depth d_{eff} , defined as the area A of the overlap between the two particles divided by the contact length l . This force is also proportional to the Young's modulus of elasticity E .

Therefore, the repulsive normal force R_{\perp} can be written as

$$R_{\perp} = Ed_{eff} = E \frac{A}{l}$$

The contact length l is defined using on the distances between the centres of mass and the force points r_i and r_j as

$$l = \frac{r_i r_j}{r_i + r_j}$$

We use a fixed value of Young's modulus $E = 10^7 N/m$ for each particle.

Besides this most key feature of assemblies of granular particles, the repulsive normal force, another important feature is the dissipation of energy which occurs due to the inter-particle collisions. The formulation of the dissipative part of the force depends on the mechanism of damping. Since we are interested to simulate static arrangements of particles, it is useful to use viscous damping in order to reach the steady state quickly. The dissipative normal force D_{\perp} is proportional to the effective interpenetration velocity d_{eff} , with a damping constant γ which gives the strength of the damping.

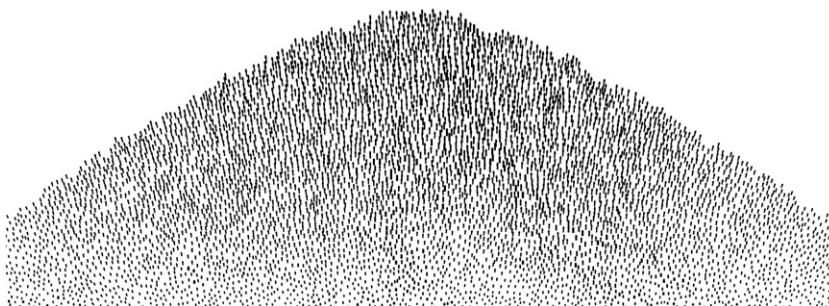


Fig. 12. Movement of the individual particles of the sand pile constructed from a point source under gravity reduction. Sand pile was relaxed by reducing gravity slowly by about 10%.

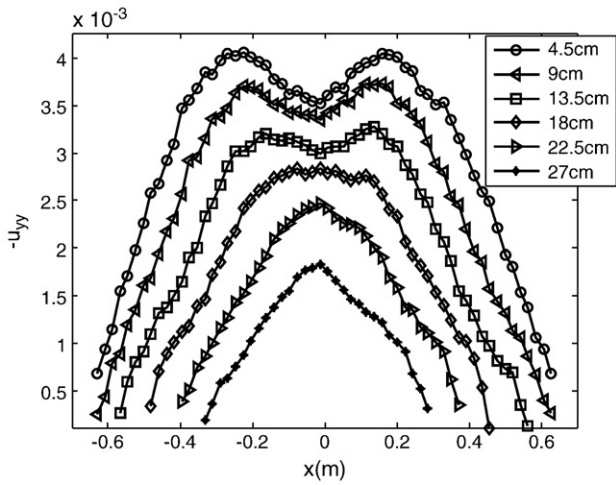


Fig. 13. Vertical normal strain distribution u_{yy} at different heights of simulated sand pile constructed from a point source.

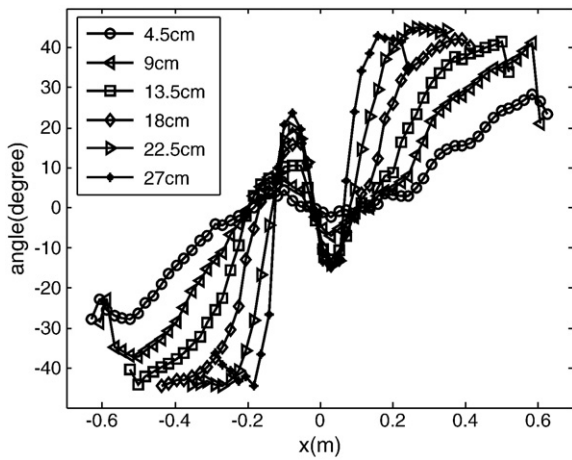


Fig. 14. Orientation of strain tensor inside the sand piles.

So the dissipative normal force can be written as

$$D_{\perp}^* = \gamma \dot{d}_{eff} \sqrt{Em_{\perp}}$$

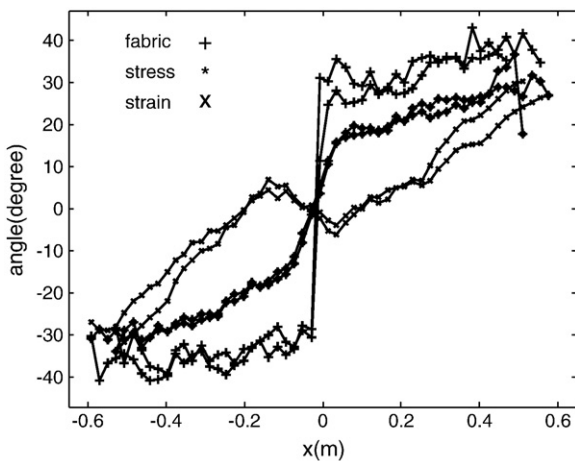


Fig. 15. Orientation of fabric, stress and strain plotted only for the first two bottom layers of the sand pile.

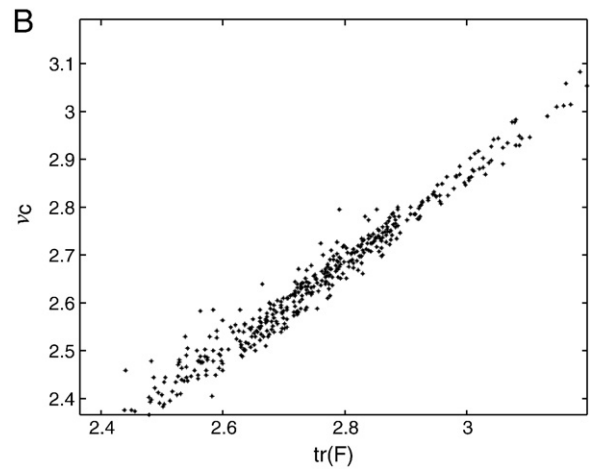
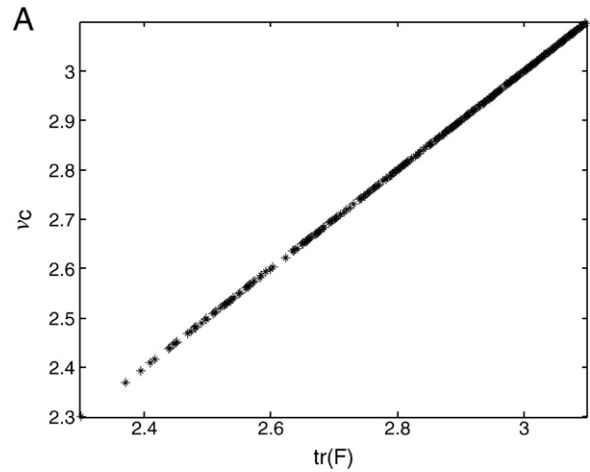


Fig. 16. Product of the volume fraction and mean coordination number plotted as a function of the trace of the averaged fabric tensor. A: for piles consisting of mono-disperse mixture of particles, B: for piles consisting of poly-disperse mixture of particles.

where the effective mass m_{\perp} of the two particles is calculated from

$$m_{\perp} = \frac{m_i m_j}{m_i + m_j}$$

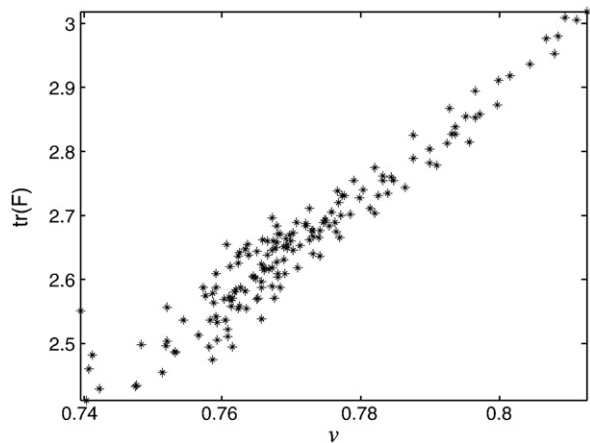


Fig. 17. Trace of the fabric tensor plotted as a function of the volume fraction for a sand pile constructed from a point source.

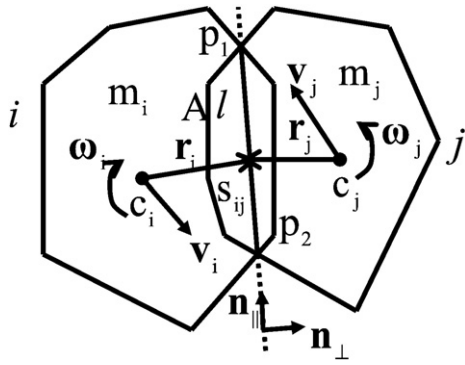


Fig. 18. Illustration of the geometry used in the calculation of the forces acting on particle *i* in contact with particle *j*.

and the effective interpenetration velocity is given by

$$\dot{d}_{eff} = \frac{\Delta A}{\Delta t} / l,$$

with $\frac{\Delta A}{\Delta t}$ is the change of contact area per time.

Actually, the dissipative normal force D_{\perp}^* is taken as the damping force D_{\perp} only as long as its combination with R_{\perp} does not lead to an attraction of the particles (which could happen during the time when the distance between the particle increases after a collision and \dot{d}_{eff} becomes negative). If that would happen D_{\perp}^* is cut off at the value $-R_{\perp}$, that means one has to make sure that the damping cannot become larger than the repulsive normal force in the case of separating particles, otherwise we might have unphysical oscillations of the separating particles. Therefore, the damping force in the normal direction D_{\perp} is given by

$$D_{\perp} = \begin{cases} D_{\perp}^* & \text{for approach} \\ \max(D_{\perp}^*; -R_{\perp}) & \text{for separation.} \end{cases}$$

A.2. Tangential force

We need to model friction which leads to a tangential force along the contact line. This is done following the ideas of Cundall and Strack. Coulomb friction forces have a definite relationship with the normal force only for sliding contacts. As long as the relative tangential velocity of the particles is zero during contact of two particles, the Coulomb friction force takes a value between zero and its maximal value $\mu F_{\perp}(t)$. A behaviour similar to this desired one is mimicked in the simulation by assigning a spring to each newly established contact. This spring is stretched during the subsequent relative motion of the two particles and exerts an increasing force, until the Coulomb friction is fully activated. Afterwards, the spring does not extend further, it is just moved along with the particles, and the friction coefficient takes its value for sliding friction, which in most of the simulations is taken equal to that for static friction.

The relative tangential velocity V_{\parallel} of two particles is obtained according to

$$V_{\parallel} = \left((v_i - v_j + r_i \times \omega_i - r_j \times \omega_j) \cdot n_{\parallel} \right) n_{\parallel},$$

where v_i and v_j are the velocities of the particles *i* and *j* and ω_i and ω_j denote their angular velocities.

So at the beginning of the collision, the tangential force is zero, and it then is adapted after each time step according to

$$F_{\parallel}(t + \Delta t) = \pm \min \left[\left| F_{\parallel}(t) + v_{\parallel} \Delta t \frac{2}{7} E + v_{\parallel} \sqrt{\frac{2}{7} E m_{\parallel}} \right|; \left| \mu F_{\perp}(t) \right| \right].$$

Herein, m_{\parallel} is the reduced mass of the two particles which includes the mass and moments of inertia of the particles, given by $m_{\parallel} = \frac{1}{\frac{1}{m_i} + \frac{1}{m_j} + \frac{r_i^2}{I_i} + \frac{r_j^2}{I_j}}$, and a viscous term (the square root term) has been added to inhibit unphysical tangential oscillations. The sign \pm is determined by the sign of the first term inside absolute value bars.

In the case of granular media, this idea of universality leads to the paradigm that for dynamical simulations even the shape of the particles does not play any role, if one makes sure by poly-disperse granulates that there is sufficient disorder. For statics, it may be important that the shape is noncircular, but all else that matters is that there are enough geometric constraints to render the simulation comparable with reality, the detailed realization of shape diversity of the particles should not matter. Moreover, it is important to have some realization of friction, otherwise one will not obtain the correct angle of repose, but whether this is implemented via Cundall–Strack springs or some other clever device (which microscopically does not precisely reproduce Coulomb's law), should be unimportant.

References

- [1] J.P. Wittmer, M.E. Cates, P. Claudin, Stress propagation and arching in static sand piles, *J. Phys. I France* 7 (1997) 39–80.
- [2] A.K. Didwania, F. Cantelaube, J.D. Goddard, Static multiplicity of stress states in granular heaps, *Proc. R. Soc. Lond. A* 456 (2000) 2569–2588.
- [3] J.P. Wittmer, M.E. Cates, P. Claudin, J.-P. Bouchaud, An explanation for the stress minimum in sand piles, *Nature* 382 (1996) 336–338.
- [4] A. P. F. Atman, P. Brunet, J. Geng, G. Redydellet, P. Claudin, R. P. Behringer, and E. Clement, From the stress response function (back) to the sand pile dip. *Eur. Phys. J. E* 17 (2005), 93–100.
- [5] J. Smid, J. Novosad, Pressure Distribution under Heaped Bulk Solids, *Proc. Powtech, Conf., Ind. Chem. Eng. Symposium Series*, 63, 1981, D3/V/1–12.
- [6] R. Brockbank, J.M. Huntely, R. Ball, Contact force distribution beneath a three dimension-al granular pile, *J. Phys. II (France)* 7 (1997) 1521–1532.
- [7] L. Vanel, D. Howell, D. Clark, R.P. Behringer, E. Clement, Memories in sand: experimental tests of construction history on stress distributions under sand piles, *Phys. Rev. E* 60 (1999) R5040.
- [8] I. Zuriguel, T. Mullin, J.M. Rotter, Effect of particle shape on the stress dip under a sand pile, *Phys. Rev. Lett.* 98 (2007) 028001.
- [9] P.A. Cundall, O.D.L. Strack, A discrete numerical model for granular assemblies, *Géotechnique* 29 (1979) 47–65.
- [10] C.W. Gear, *Numerical Initial Value Problems in Ordinary Differential Equations*, Prentice Hall, 1971.
- [11] A. Schinner, Ein Simulationssystem für granulare Aufschüttungen aus Teilchen variabler form. PhD thesis, Univ. Magdeburg, 2001.
- [12] B. Cambou, M. Chaze, F. Dedecker, Change of scale in granular materials, *Eur. J. Mech. A Solids* 19 (2000) 999–1014.
- [13] J.D. Goddard, Continuum Modeling of Granular Assemblies, in: H.J. Herrmann, J.P. Hovi, S. Luding (Eds.), *Physics of Dry Granular media*, Kluwer Academic Publishers, Dordrecht, 1998, pp. 1–24.
- [14] S.C. Cowin, A Simple Theory of Instantaneously Induced Anisotropy, in: J.T. Jenkins, M. Satake (Eds.), *Micro-mechanics of granular materials*, Elsevier, Amsterdam, 1988, pp. 71–80.
- [15] M.H. Sadd, J. Gao, A. Shukla, Numerical analysis of wave propagation through assemblies of elliptical particles, *Comput. Geotech.* 20 (3/4) (1997) 323–344.
- [16] J. D. Goddard, Micro-structural origins of continuum stress fields—a brief history and some unresolved issue. In: D. Dekee, P. N. Kaloni, (Eds.) *Recent developments in structured continua*. Pitman research notes in Mathematics No. 143, Longman. J. Wiley, New York, p. 179, 1986.
- [17] M.M. Mehrabadi, S. Nemat-Nasser, H.M. Shodja, G. Subhash, Some basic theoretical and experimental results on micromechanics of granular flow, *Micromech. Granular Media*, Elsevier, Amsterdam, 1988.
- [18] C.S. Chang, *Micromechanical modeling of constitutive relations for granular media*, *Micromech. Granular media*, Elsevier, Amsterdam, 1988.
- [19] C. Thornton, C.W. Randall, *Applications of Theoretical Contact Mechanics to Solid Particle System Simulation*, *Micromech. Granular media*, Elsevier, Amsterdam, 1988.
- [20] R. Blumenfeld, Stress in isostatic granular systems and emergence of force Chains, *Phys. Rev. Lett.* 93 (2004) 10.
- [21] M. Madadi, O. Tsoungui, M. Lätzel, S. Luding, On the fabric tensor of poly-disperse granular materials in 2D, *Int. J. Solids Struct.* 41 (2004) 2563–2580.